HEAT-UP AND COOL-DOWN TEMPERATURE-DEPENDENT HYDRIDE REORIENTATION BEHAVIORS IN ZIRCONIUM ALLOY CLADDING TUBES

JU-JIN WON, MYEONG-SU KIM, and KYU-TAE KIM*
Dongguk University, Nuclear & Energy System Engineering Dept., 707 Seokjang-Dong, Gyeongju, Gyeongbuk 780-714 Korea
*Corresponding author. E-mail : ktkim@dongguk.ac.kr

Hydride reorientation behaviors of PWR cladding tubes under typical interim dry storage conditions were investigated with the use of as-received 250 and 485ppm hydrogen-charged Zr-Nb alloy cladding tubes. In order to evaluate the effect of typical cool-down processes on the radial hydride precipitation, two terminal heat-up temperatures of 300 and 400ºC, as well as two terminal cool-down temperatures of 200 and 300ºC, were considered. In addition, two cooling rates of 2.5 and 8.0ºC/min during the cool-down processes were taken into account along with zero stress or a tensile hoop stress of 150MPa. It was found that the 250ppm hydrogen-charged specimen experiencing the higher terminal heat-up temperature and the lower terminal cool-down temperature generated the highest number of radial hydrides during the cool-down process under 150MPa hoop tensile stress, which may be explained by terminal solid hydrogen solubilities for precipitation, and dissolution and remaining circumferential hydrides at the terminal heat-up temperatures. In addition, the slower cool-down rate generates the larger number of radial hydrides due to a cooling rate-dependent, longer residence time at a relatively high temperature that can accelerate the radial hydride nucleation and growth.

KEYWORDS : Zirconium Alloy Tube, Spent Nuclear Fuel, Radial Hydride, Circumferential Hydride, Terminal Solid Solubility

1. INTRODUCTION

The usage of PWR fuel claddings may be limited by the degradation of mechanical properties caused by excessive hydrides in the fuel claddings, and their brittle cracking behaviors [1-4]. During the interim dry storage, the hydride embrittlement of the zirconium alloy claddings such as Zircaloy-4, Zirlo, M5 and HANA may be governed by the number of radial hydrides in the claddings precipitated during the cool-down and their morphologies [5-13]. Therefore, the hydride platelets in the claddings need to be mainly oriented in the circumferential direction to reduce such hydride embrittlement. It is reported that the hydride reorientation from the circumferential to the radial direction is to a large extent determined by the texture of the cladding tubes [14-16].

It is well known that the cladding tube pilger processes provide optimized cladding textures generating mostly circumferential hydrides under compressive hoop stress or no stress conditions. During the interim dry storage of the high burnup fuel rods, however, relatively high hoop tensile stresses and heat-up temperatures may occur on the cladding tubes, because the claddings are allowed to be heated up to a certain terminal temperature less than 400ºC when the spent fuel rods are transferred from the

wet storage pit to the interim dry storage cask. The already existing circumferential hydrides in the spent fuel claddings may be dissolved during such heat-up processes. Then, the dissolved hydrogen atoms may precipitate mainly in the radial direction during the cool-down process in the interim dry storage cask, only if the hoop tensile stress on the cladding is larger than a certain threshold stress for radial hydride precipitation, which was reported to be about 90MPa in the temperature range of between 250 and 550ºC [17-18]. However, the number of the radial hydrides precipitated during the cool-down process depends on terminal heat-up temperatures, terminal cool-down temperatures, terminal solid solubilities for precipitation and dissolution, hoop tensile stresses, cooling rates, initial hydrogen contents and the number of thermal cycles.

Based on the current license requirements for the PWR fuel rod loading into the reactor core, the hydrogen content in the cladding is to be less than 600ppm on the one hand, and the fuel rod internal pressure is to be less than the reactor coolant system pressure (15.5MPa) on the other hand, which results in a compressive hoop stress on the cladding during the in-reactor operation. During the interim dry storage, however, a maximum hoop tensile stress on the cladding tube may be 150MPa that can be calculated with the allowable rod internal pressure of 15.5MPa and

the atmospheric pressure on the outer rod surface. It is reported that the fuel cladding temperatures during interim dry storage may decrease by about 100ºC per 10 years (2×10^{-5}ºC/min) [19]. In this study, therefore, as-received 250ppm hydrogen-charged (250ppm-H) and 485ppm hydrogen-charged (500ppm-H) Zr-Nb alloy cladding tubes were employed with terminal heat-up temperatures of 300 and 400ºC, terminal cool-down temperatures of 200 and 300ºC, cooling rates of 2.5 and 8.0ºC/min, and zero and 150MPa hoop tensile stresses, in order to evaluate the effect of various cool-down processes on the number of radial hydride precipitation and hydride configurations.

2. EXPERIMENTAL SETUP

Table 1 summarizes the chemical compositions, textures and dimensions of the Zr-Nb alloy cladding tubes. The cladding tubes used in this study, that were supplied by Korea Electric Power Company Nuclear Fuel Company (KNF), were heat-treated to be in a stress-relieved condition. To make a final cladding tube, the typical three-step pilger process, starting from the Tube Reduced Extrusion (TREX), were employed by KNF. Two target values for the hydrogen contents in the Zr-Nb alloy cladding tubes were considered to be 250 and 500ppm. The as-received Zr-Nb alloy cladding tubes containing 10ppm hydrogen atoms were cut into several parts of 100mm each and then their surfaces were cleaned with acetic acid. The two parts were charged with hydrogen for a certain time (e.g., 24 hours for 250ppm-H tubes) in the vacuum furnace at 400ºC containing a mixture gas of hydrogen (150torr) and helium (200torr) to generate a uniform distribution of hydrogen atoms through the tubes [20]. It should be noted that the temperature uncertainty of the vacuum furnace is within ±5ºC. The hydrogen contents of the test specimens were analyzed by the LECO hydrogen analyzer RH600. Two kinds of final hydrogen contents in the hydrogen-charged specimens were measured to be in the range of 250±25ppm and 485±25ppm, respectively.

Hydrogen-charged cladding tubes were cut transversely to make ring specimens of 5 mm in width. Axial sections of ring specimens before and after the heat-up and the cool-down processes were examined by an optical microscopy to reveal hydride dissolution and precipitation behaviors along with its configurations. The etchant used for the met-allographic examinations was composed of HF, HNO_3, and H_2O in a volume ratio of 10:45:45. Fig. 1 shows a schematic configuration of the ring test specimen, and two half-cylinder loading pins that strain the ring test specimen. The diameter of the half-cylinder loading pin is 8.35mm and the gage length of the test specimens is 2mm. Special grips were designed and fabricated to fix the loading pins and apply a certain load on the ring test specimen.

In this study, five cases of hydride reorientation tests were carried out. First of all, as shown in Fig. 2a, the specimens were heated up at a rate of 2.5ºC/min from room temperature (25ºC) (refer to H^0_R) to two respective heat-up temperatures of 200 and 300ºC under zero hoop stress (refer to H^0_2 and H^0_3) to investigate the hydride dissolution behaviors and subsequent mechanical property variations of the Zr-Nb claddings. The specimens heated up to 200 or 300ºC were water-quenched to freeze the hydride distribution at those heat-up temperatures. However, some specimens heated up to 300ºC were solution-annealed at that temperature for 2 hours, as shown in Fig. 2a. Then, those specimens were cooled down to 200ºC with the cooling rate of 2.5ºC/min under zero hoop stress (refer to C^0_{32F}) to investigate the effects of zero hoop tensile stress, initial hydrogen content, and terminal cool-down temperature on the number of radial and circumferential hydrides precipitated, and on the hydride configurations. Secondly, as shown in Fig. 2b, the specimens were heated up at a rate of 2.5ºC/min from room temperature (refer to H^s_R) to two respective terminal heat-up temperatures of 200 and 300ºC under 150MPa hoop tensile stress (refer to H^s_2 and H^s_3). The specimens were solution-annealed at the terminal heat-up temperature for 2 hours prior to cool-down, as shown in Fig. 2b. Then, those specimens were cooled down to 200ºC with the cooling rate of 2.5ºC/min under the 150MPa hoop tensile stress (refer to C^s_{32F}) to investigate the effects of hoop tensile stress, initial hydrogen content, and terminal cool-down temperature on the number of radial and circumferential hydrides precipitated, and on the hydride configurations.

Thirdly, as shown in Fig. 3a, the specimens were heated up with the heating rate of 2.5ºC/min from room temperature to one terminal heat-up temperature of 400ºC under zero hoop stress (refer to H^0_4) to investigate the hydride dissolution behaviors and subsequent mechanical property

Table 1. Summary of Zr-Nb Alloy Cladding Data Used in This Work

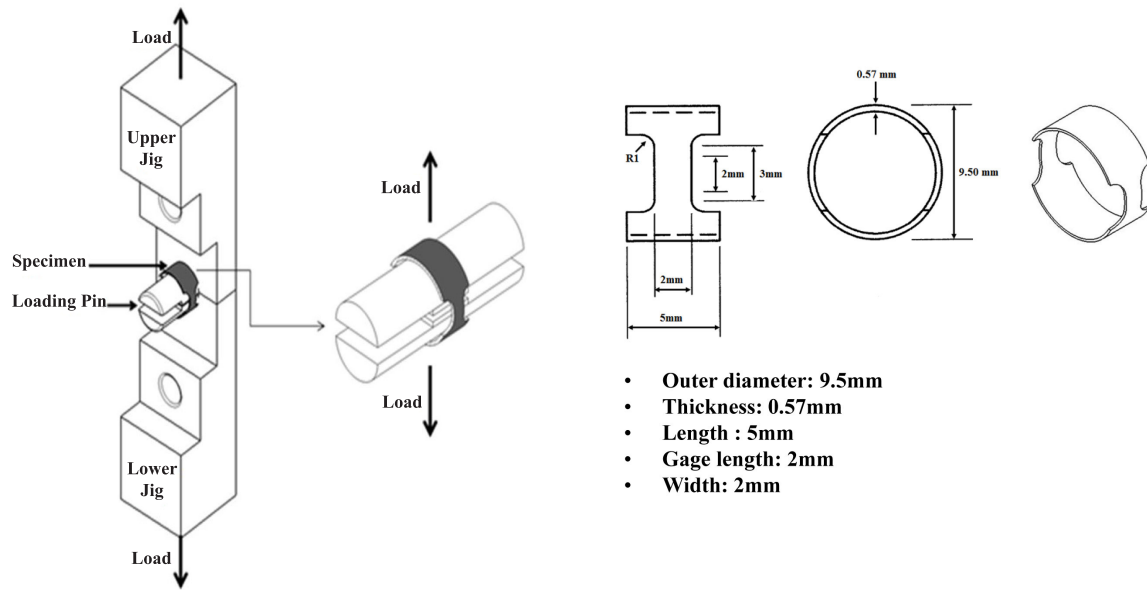| Cladding materials	Chemical composition (w/o)	Texture (Kearns number)	Tube dimension (mm)
Zr-Nb alloy	Zr-1.0Nb-1.0Sn-0.1Fe	f_r (radial) = 0.62 f_t (tangential) = 0.26 f_a (axial) = 0.12	Outer dia. = 9.50 Thickness = 0.57

- Outer diameter: 9.5mm
- Thickness: 0.57mm
- Length : 5mm
- Gage length: 2mm
- Width: 2mm

Fig. 1. Configurations of a Ring Tensile Test Specimen and Loading Pins.

a) zero stress condition

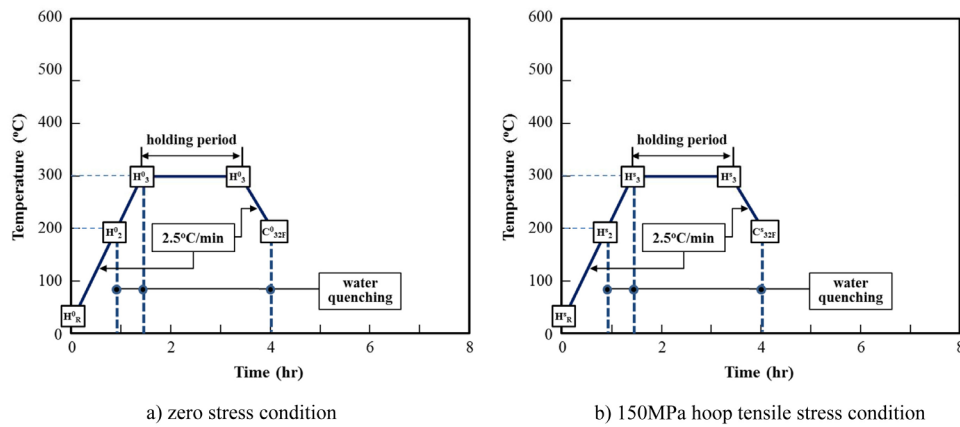b) 150MPa hoop tensile stress condition

Fig. 2. Schematic Diagrams of Heat-up to 300°C and Cool-down Processes form 300 to 200oC under Zero Stress and 150MPa Hoop Tensile Stress Conditions.

a) zero stress condition
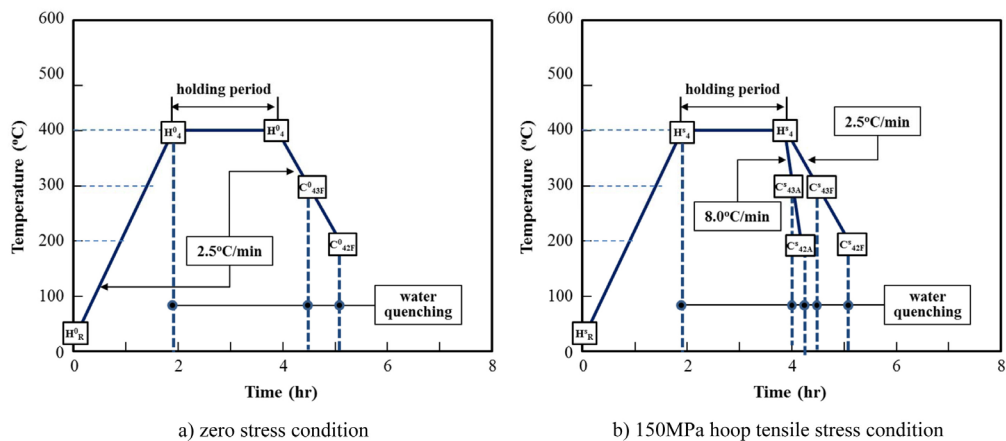
b) 150MPa hoop tensile stress condition

Fig. 3. Schematic Diagrams of Heat-up to 400°C and Cool-down Processes from 400 to 300 and 200oC under Zero Stress and 150MPa Hoop Tensile Stress Conditions.

variations of the Zr-Nb claddings. The specimens were solution-annealed at that heat-up temperature for 2 hours, as shown in Fig. 3a. Then, those specimens were cooled down to 300 and 200ºC, respectively, with the cooling rate of 2.5ºC/min under zero hoop stress (refer to C^0_{43F} and C^0_{42F}) to investigate the effects of zero hoop tensile stress, initial hydrogen content, and terminal cool-down temperature on the number of radial and circumferential hydrides precipitated, and on the hydride configurations.

Fourthly, as shown in Fig. 3b, the specimens were heated up at a rate of 2.5ºC/min from room temperature to one terminal heat-up temperatures of 400ºC under the 150MPa hoop tensile stress (refer to H^s_4). The specimens were solution-annealed at that heat-up temperature for 2 hours, as shown in Fig. 3b. Then, those specimens were cooled down to 300 and 200ºC, respectively, with the cooling rate of 2.5ºC/min under the 150MPa hoop tensile stress (refer to C^s_{43F} and C^s_{42F}) to investigate the effects of hoop tensile stress, cooling rate, initial hydrogen content and terminal cool-down temperature on the number of radial and circumferential hydrides precipitated, and on the hydride configurations.

Finally, as shown in Fig. 3b, the solution-annealed specimens at 400ºC were cooled down to 300 and 200ºC, respectively, with the cooling rate of 8.0ºC/min under the 150MPa hoop tensile stress (refer to C^s_{43A} and C^s_{42A}) to investigate the effects of hoop tensile stress, cooling rate, initial hydrogen content, and terminal cool-down temperature on the number of radial and circumferential hydrides precipitated, and on the hydride configurations.

To check the reproducibility of the test results, the heat-up and cool-down tests, along with the microstructure examinations, were repeated twice using the same batch of the test specimens.

3. RESULTS AND DISCUSSION

3.1 Heat-up Tests

The as-received 250ppm-H and 485ppm-H ring specimens were heated up from room temperature (H^0_R and H^s_R in Figs. 2 and 3) to the respective heat-up temperatures of 200, 300 and 400ºC under the zero stress condition (refer to H^0_R, H^0_2, H^0_3 and H^0_4 in Figs. 2 and 3) and the 150MPa hoop tensile stress condition (refer to H^s_R, H^s_2, H^s_3 and H^s_4 in Figs. 2 and 3). Microstructures of the specimens were examined at 25, 200, 300 and 400ºC by an optical microscopy to reveal the hydride dissolution behavior, the number of remaining circumferential hydrides and their configurations.

It was found that there exists no effect of the hoop tensile stress on the remaining circumferential hydrides and their configurations for the 250ppm-H and 485ppm-H specimens. The optical micrographs for the heat-up tests shown in Fig. 4 indicate that all the hydrides appear to be oriented in the circumferential direction, regardless of the heat-up temperatures, and the higher heat-up temperature generated the fewer hydrides. This shows that the hydride dissolution is increased with the increase in temperature. In detail, the circumferential hydride platelets became shorter and thinner with the increase in temperature. This hydride dissolution behavior can be easily explained by the terminal solid solubility for dissolution [21], as shown in Fig. 5. The solid curve shown in this figure, illustrates the hydrogen solid solubilities for dissolution at 25, 200, 300 and 400ºC are about 3, 20, 80 and 240ppm, respectively. From these hydrogen solid solubilities for dissolution, it can be seen that very few hydrides are dissolved even at the terminal heat-up temperature
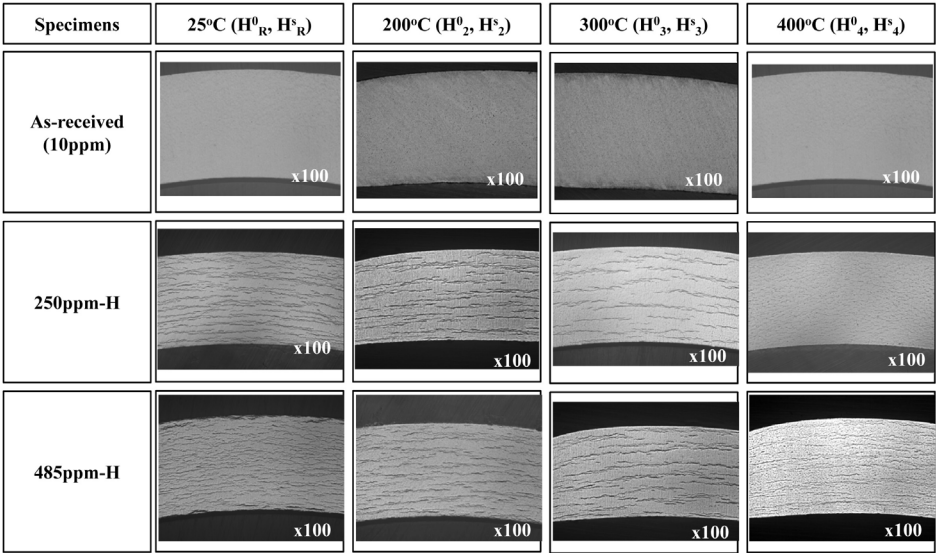
Specimens	25ºC (H^0_R, H^s_R)	200ºC (H^0_2, H^s_2)	300ºC (H^0_3, H^s_3)	400ºC (H^0_4, H^s_4)
As-received (10ppm)	x100	x100	x100	x100
250ppm-H	x100	x100	x100	x100
485ppm-H	x100	x100	x100	x100

Fig. 4. Hydride Distributions Generated from the Heat-up Processes with 2.5ºC/min.

of 200 and 300ºC. Despite the hydrogen solid solubility for dissolution at 400ºC is about 240ppm, nearly all the hydrides are dissolved into hydrogen atoms for the 250ppm-H specimen at 400ºC, whereas about half of the circumferential hydrides are dissolved for the 485ppm-H specimen.

3.2 Cool-down Tests under Zero Stress Condition

The as-received 250ppm-H and 500ppm-H ring specimens were cooled down under the zero stress condition with a cooling rate of 2.5ºC/min from the terminal heat-up temperature of 300ºC (H^0_3) to the terminal cool-down temperature of 200ºC (C^0_{32F}) on the one hand, and from the terminal heat-up temperature of 400ºC (H^0_4) to the two terminal cool-down temperature of 300 and 200ºC (C^0_{43F} and C^0_{42F}) on the other hand. The cool-down specimens were water quenched at the respective cool-down temperatures to freeze their microstructures at that point.

The microstructures of the cool-down specimens were examined by an optical microscopy to reveal the number of hydrides and their configurations. The optical micrographs of the cool-down specimens shown in Fig. 6 indicate that circumferential hydrides only were generated during the cool-down, but the number of the circumferential hydrides at each cool-down temperature appears to be smaller than that at the corresponding heat-up temperatures. This may be explained by the terminal solid solubilities for dissolution and precipitation, as well as a critical hoop tensile stress for radial hydride precipitation during the cool-down process. From Fig. 5, it can be seen that the terminal solid solubilities for precipitation at 400, 300 and 200ºC are 350, 150 and 50ppm, respectively, while those for dissolution at 400, 300 and 200ºC are 240, 80 and 20ppm, respectively. Obviously, the terminal solid solubilities for precipitation are larger than the terminal solid solubilities for dissolution, resulting in a lower number of hydrides during the precipitation at the respective cool-down temperatures. Furthermore, it is reported that hydrides will be precipitated in the radial direction during the cool-down process only if the hoop tensile stress on the zirconium cladding is larger than a certain threshold stress for radial hydride precipitation, which was reported to be about 90MPa in the temperature range of between 250 and 550ºC [17-18]. Therefore, the cool-down tests under zero stress condition cannot generate radial hydrides during the respective cool-down processes, as expected.
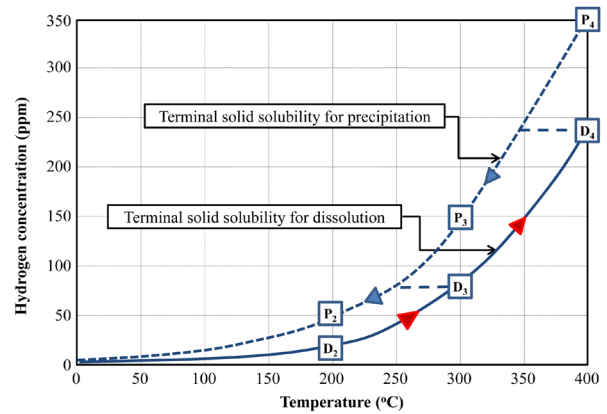

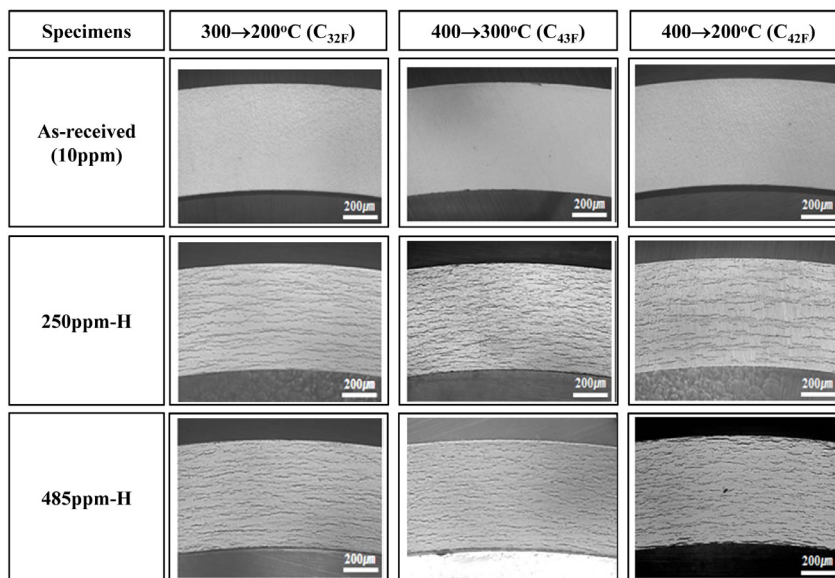Fig. 5. Terminal Solid Solubility of Hydrogen in Zircaloy Claddings.

Fig. 6. Hydride Distributions Generated from the Cool-down Processes with 2.5ºC/min and Zero Stress Condition.

3.3 Cool-down Tests under 150MPa Hoop Tensile Stress Condition

Three cases of the cool-down processes under the 150MPa hoop tensile stress condition were investigated in this study. Firstly, the as-received, 250ppm-H and 500ppm-H ring specimens were cooled down at a rate of 2.5°C/min from the terminal heat-up temperature of 300°C (H_3^s) to the terminal cool-down temperature of 200°C (C_{32F}^s), as shown Fig. 2b. Secondly, they were cooled down with the cooling rate of 2.5°C/min from the terminal heat-up temperature of 400°C (H_4^s) to the terminal cool-down temperatures of 300 and 200°C (C_{43F}^s and C_{42F}^s), as shown in Fig. 3b. Finally, they were cooled down with the cooling rate of 8.0°C/min from the terminal heat-up temperature of 400°C (H_4^s) to the terminal cool-down temperatures of 300 and 200°C (C_{43A}^s and C_{42A}^s), as shown in Fig. 3b.

Fig. 7 shows the optical micrographs for the cool-down processes from 300 to 200°C (first case) and from 400 to 300 and 200°C with the cooling rate of 2.5°C/min (second case). From this figure, it can be seen that C_{42F}^s for the 250 and 485ppm-H specimens generated the highest number of radial hydrides precipitated during the cool-down, whereas C_{32F}^s for the 250 and 485ppm-H specimens generated the lowest number of radial hydrides. The hydrides shown in this figure are classified into circumferential and radial hydrides. The former is defined as the platelets oriented within 0~40° to the circumferential axis, whereas the latter are oriented within 50~90° to the circumferential axis. The small fraction of hydrides within 40~50° to the circumferential axis are not counted as either radial or circumferential hydrides. On the other hand, the fraction of the radial hydrides may be defined as the length ratio of the radial hydrides to the total hydrides precipitated during the cool-down. In other words, the remaining circumferential hydrides at 400°C for the 500ppn-H specimens are not taken into account for the calculation of the radial hydride fraction.

Fig. 8 shows the radial hydride fractions for the 250 and 485ppm-H specimens cooled down from 400 to 300 and 200°C. The fractions for the 250 and 485ppm-H specimens cooled down from 300 to 200°C are below 2%, which are not shown in Fig. 8. The variations in the radial hydride fractions may be explained by the difference in the terminal solid solubilities for dissolution and precipitation. It should be noted that the number of the hydrogen atoms to be precipitated during the cool-down processes of C_{42F}^s, C_{43F}^s and C_{32F}^s are calculated to be 190, 90 and 30ppm, respectively, from the data given in Fig. 5.
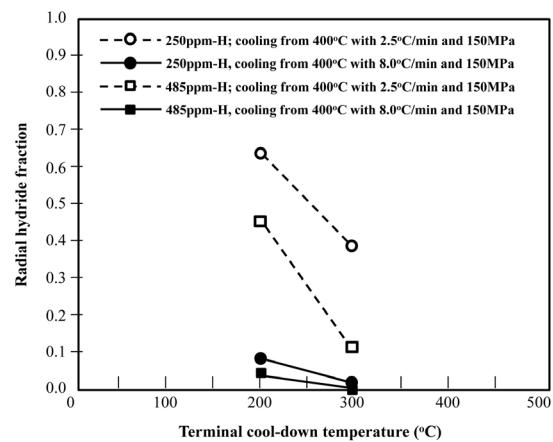

Fig. 8. Radial Hydride Fraction Generated from the Cool-down Processes from 400°C with 2.5 and 8.0°C/min under 150MPa Hoop Tensile Stress Condition.
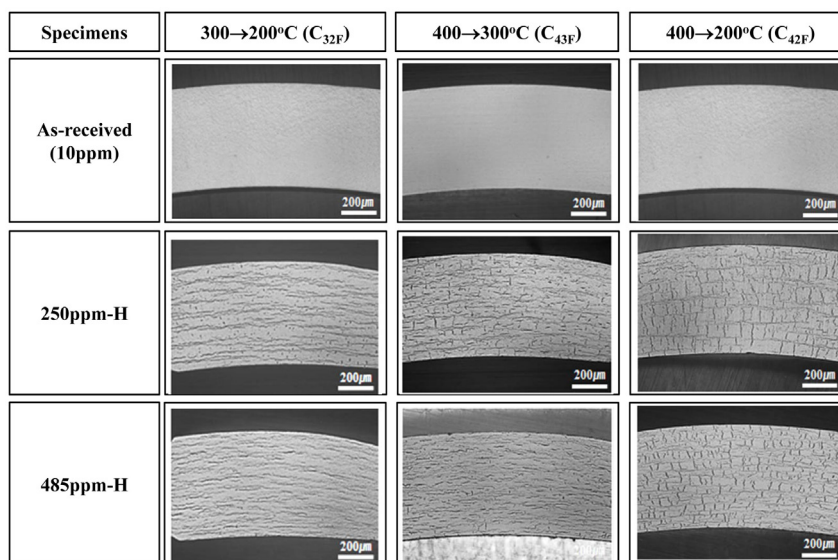

Fig. 7. Hydride Distributions Generated from the Cool-down Processes with 2.5°C/min and 150MPa Hoop Tensile Stress Condition.

The 485ppm-H specimens generated relatively fewer and shorter radial hydrides than the 250ppm-H specimens. This may occur because the remaining circumferential hydrides in the 485ppm-H specimens at the terminal heat-up temperatures played an active role as hydride nucleation sites during the hydride precipitation with the dissolved hydrogen atoms. That is to say, more remaining circumferential hydrides will generate more circumferential hydrides precipitated during the cool-down. In addition, the length of the radial hydrides formed in the 485ppm-H specimens is relatively shorter than those formed at 250ppm-H, since the remaining circumferential hydrides may block the growth of radial hydrides.

Fig. 9 shows the optical micrographs for the cool-down processes from 400 to 300 and 200ºC with the cooling rate 8.0ºC/min (third case). From this figure, it can be seen that C^s_{42A} generated relatively larger number of radial hydrides precipitated during the cool-down than C^s_{43A}, which became more significant for the 250ppm-H specimens. This may be caused by the difference in the terminal solid solubilities for dissolution and precipitation, as well as the remaining circumferential hydrides in the 485ppm-H specimens, as described above. It should be noted that the numbers of the hydrogen atoms to be precipitated during the cool-down processes of C^s_{42A} and C^s_{43A} are calculated to be 190 and 90ppm, respectively, from the data given in Fig. 5.

As shown in Fig. 8, however, the radial hydride fractions precipitated during the cool-down with the cooling rate of 8.0ºC/min is much smaller than those with the cooling rate of 2.5ºC/min. In addition, the lengths of the radial hydrides with the cooling rate of 8.0ºC/min are

much shorter than those with the cooling rate of 2.5ºC/min. This phenomenon may be explained by the residence time at a relatively higher temperature during the cool-down. The hydrogen atoms may precipitate preferentially in the radial direction when the tensile hoop stress applied is larger than a threshold stress for the radial hydride formation, and the probability for the radial hydride precipitation increases with a longer residence time at a relatively higher temperature, due to a sufficient time for searching out the radial hydride nucleation sites. As mentioned above, the cooling rate of 2.5ºC/min generated relatively larger radial hydride fractions and the longer radial hydrides than the cooling rate of 8.0ºC/min, since the former provides a longer residence time at a relatively higher temperature.

4. CONCLUSIONS

This study investigated the effects of terminal heat-up temperatures, terminal cool-down temperatures, cooling rates, hoop tensile stresses and hydrogen contents in the cladding on the number of the radial hydrides precipitated during the cool-down and their configurations. The major results obtained in this study may be summarized as follows:

1) The heat-up processes indicate that all the hydrides were oriented in the circumferential direction, regardless of the terminal heat-up temperatures and hoop stress conditions, and that the hydride dissolution was increased, and the circumferential hydride platelets became shorter and thinner, with the increase in temperature.

2) The cool-down processes under the zero hoop stress condition indicate that the hydrides were precipitated only in the circumferential direction, but the number of the circumferential hydrides at each cool-down temperature is lower than those at the corresponding heat-up temperatures. This phenomenon may be explained by the terminal solid solubilities for precipitation and dissolution in one case, and by a critical hoop tensile stress for radial hydride precipitation during the cool-down process in the other case.

3) The cool-down processes under the 150MPa hoop tensile stress condition indicate that the 250ppm-H specimens generated larger radial hydride fractions than the 485ppm-H specimens, the 2.5ºC/min cooling rate provided larger radial hydride fractions and longer radial hydrides than the 8.0ºC/min cooling rate, and the radial hydride fraction was increased very sharply during the cooling period from 300 to 200ºC when cooled down from the terminal heat-up temperature of 400ºC with the 2.5ºC/min cooling rate. The aforementioned phenomena may be explained by the remaining circumferential hydrides for the 485ppm-H specimens, the residence time at a
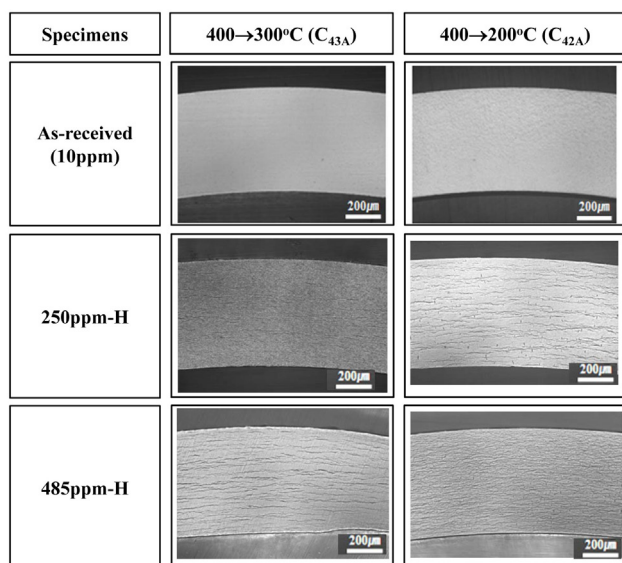

Specimens	400→300ºC (C_{43A})	400→200ºC (C_{42A})
As-received (10ppm)		
250ppm-H		
485ppm-H		

Fig. 9. Hydride Distributions Generated from the Cool-down Processes with 8.0ºC/min and 150MPa Hoop Tensile Stress Condition.

relatively higher temperature during the cool-down process, and the terminal solid solubilities for precipitation and dissolution.

REFERENCES

[1] S. Kim, Y. Kwon and Y. Kim, "The Effect of Texture Variation on Delayed Hydride Cracking Behavior of Zr–2.5%Nb Plate," *J. Nucl. Mater*. vol. 273, pp. 52-59 (1999).

[2] A. Varias and A. Massih, "Simulation of Hydrogen Embrittlement in Zirconium Alloys under Stress and Temperature Gradients ," *J. Nucl. Mater*. vol. 279, pp. 273-285 (2000).

[3] G. Bertolino, G. Meyer, and J., Perez Ipina, "Effects of Hydrogen Content and Temperature on Fracture Toughness of Zircaloy-4," *J. Nucl. Mater*. vol. 320, pp. 272-279 (2003).

[4] K. Une and S. Ishimoto, "Dissolution and Precipitation Behavior of Hydrides in Zircaloy-2 and High Fe Zircaloy ," *J. Nucl. Mater*. vol. 322, pp. 66-72 (2003).

[5] J. Bai, J. Ni, D. Gilbon, C. Prioul and D. Francois, "Hydride Embrittlement in Zircaloy-4 Plate, II. Interaction between the Tensile Stress and the Hydride Morphology," *Metall. Mater. Trans*. vol. 25A, pp. 1199-1208 (1994).

[6] B. Cox and Y. Wong, "A Hydrogen Uptake Micro-mechanism for Zr alloys ," *J. Nucl. Mater* . vol. 270, pp.134-146 (1999).

[7] M. Kim, H. Kim, S. Min and K. Kim, "Cladding Cooling Rate-Dependent Hydride Reorientation and Configuration ," *Korean J. Met. Mater*. vol. 51, pp. 477-486 (2013).

[8] S. Min, M. Kim and K., Kim, "Cooling rate- and hydrogen content-dependent hydride reorientation and mechanical property degradation of Zr–Nb alloy claddings," *J. Nucl. Mater*. vol. 441, pp. 306-314 (2013).

[9] S. Min, M. Kim, C. Won and K. Kim, "Effects of Cooling Rates on Hydride Reorientation and Mechanical Properties of Zirconium Alloy Claddings under Interim Dry Storage Conditions," *Korean J. Met. Mater*. vol. 51, pp. 487-495 (2013).

[10] Q. Chen, J. Ostien and G. Hansen , "Development of a used fuel cladding damage model incorporating circumferential and radial hydride responses." *J. Nucl. Mater*. vol. 447, pp. 292-303 (2014).

[11] S. Hong, K. Lee and K. Kim, "Effect of the circumferential hydrides on the deformation and fracture of Zircaloy cladding tubes," *J. Nucl. Mater*. vol. 303, pp. 169-176 (2002).

[12] S. Hong and K. Lee, "Stress-induced reorientation of hydrides and mechanical properties of Zircaloy-4 cladding tubes," *J. Nucl. Mater*. vol. 340, pp. 203-208 (2005).

[13] K. Lee, Y. Choi, K. Joo, K. Kim and. S. Hong, "Reorientation of Hydrides and Its Effect on the Mechanical Properties of Zr-Nb-Sn-Fe Cladding Tubes," *J. Nucl. Sci. Tech*., vol. 42, pp. 219-224 (2005).

[14] M. Louthan Jr. and R. Marshall, "Control of Hydride Orientation in Zircaloy ," *J. Nucl. Mater*. vol. 9, pp. 170 (1963).

[15] R. Marshall, "Influence of Fabrication History on Stress-oriented Hydrides in Zircaloy Tubing," *J. Nucl. Mater*. vol. 24, pp. 34 (1967).

[16] R. Marshall and M. Louthan Jr., "Tensile Properties of Zircaloy with Oriented Hydrides ," *Trans. ASM*. vol. 56, pp. 693 (1963).

[17] H. Chung, "Understanding Hydride- and Hydrogen-related Processes in High-burnup Cladding in Spent-fuel Storage and Accident Situations ," Proceedings of the International Meeting on LWR Fuel Performance, Orlando, FL, U.S.A., pp. 470 (2004).

[18] A. Colas et al., "In-situ Study of Hydride Precipitation Kinetics and Re-orientation in Zircaloy Using Synchrotron Radiation," *Acta Mater*. vol. 58, pp. 6575 (2010).

[19] H. Kim, Y. Jeong and K. Kim, "The Effects of Creep and Hydride on Spent Fuel Integrity during Interim Dry Storage ," *Nucl. Eng. Tech*. vol. 49, pp. 249 (2010).

[20] H. Kim et al., "Evaluation of Hydride Effect on Fuel Cladding Degradation ," *Korean J. Met. Mater*. vol. 48, pp. 717 (2010).

[21] B. Kammenzind et al., "Hydrogen Pickup and Redistribution in Alpha-Annealed Zircaloy-4," International Symposium on Zirconium in the Nuclear Industry, Garmisch-Partenkirchen, Germany, Sep. 11-14, pp. 338 (1995).